



**HAL**  
open science

## How vial geometry variability influences heat transfer and product temperature during freeze-drying

Bernadette Scutella, Stéphanie Passot, Erwan Bourlés, Fernanda Fonseca, Ioan-Cristian Trelea

► **To cite this version:**

Bernadette Scutella, Stéphanie Passot, Erwan Bourlés, Fernanda Fonseca, Ioan-Cristian Trelea. How vial geometry variability influences heat transfer and product temperature during freeze-drying. *Journal of Pharmaceutical Sciences*, 2017, 106 (3), pp.770-778. 10.1016/j.xphs.2016.11.007 . hal-01465155

**HAL Id: hal-01465155**

**<https://hal.science/hal-01465155>**

Submitted on 10 Feb 2017

**HAL** is a multi-disciplinary open access archive for the deposit and dissemination of scientific research documents, whether they are published or not. The documents may come from teaching and research institutions in France or abroad, or from public or private research centers.

L'archive ouverte pluridisciplinaire **HAL**, est destinée au dépôt et à la diffusion de documents scientifiques de niveau recherche, publiés ou non, émanant des établissements d'enseignement et de recherche français ou étrangers, des laboratoires publics ou privés.

1           **How vial geometry variability influences heat transfer and product**  
2                                   **temperature during freeze-drying**

3

4 Authors: BERNADETTE SCUTELLA<sup>1,2</sup>, STEPHANIE PASSOT<sup>1</sup>, ERWAN BOURLES<sup>2</sup>,  
5 FERNANDA FONSECA<sup>1</sup>, IOAN CRISTIAN TRELEA<sup>1</sup>

6

7 <sup>1</sup> UMR GMPA, AgroParisTech, INRA, Université Paris Saclay, 78850 Thiverval-Grignon,  
8 France

9 <sup>2</sup> GSK Vaccines, Rixensart, Belgium

10

11 **ABSTRACT:** Vial design features can play a significant role in heat transfer between the  
12 shelf and the product and, consequently, in the final quality of the freeze-dried product. Our  
13 objective was to investigate the impact of the variability of some geometrical dimensions of a  
14 set of tubing vials commonly used for vaccine production on the distribution of the vial heat  
15 transfer coefficients ( $K_v$ ) and its potential consequence on product temperature. Sublimation  
16 tests were carried out using pure water and eight combinations of chamber pressure (4 to 50  
17 Pa) and shelf temperature (-40 °C and 0 °C) in two freeze-dryers.  $K_v$  values were individually  
18 determined for 120 vials located in the center of the shelf. Vial bottom curvature depth and  
19 contact area between the vial and the shelf were carefully measured for 120 vials and these  
20 data were used to calculate  $K_v$  distribution due to variability in vial geometry. At low  
21 pressures commonly used for sensitive products (below 10 Pa), the vial-shelf contact area  
22 appeared crucial for explaining  $K_v$  heterogeneity and was found to generate, in our study, a  
23 product temperature distribution of approximately 2 °C during sublimation. Our approach  
24 provides quantitative guidelines for defining vial geometry tolerance specifications and  
25 product temperature safety margins.

26

27 **Keywords:** Freeze drying/lyophilization; amorphous; drying; vaccines; distribution; vial heat  
28 transfer coefficient; sublimation rate; vial design; inter-vial heterogeneity

29

30

31

## 32 INTRODUCTION

33 Nowadays, freeze-drying is an essential and valuable preservation method to ensure the long-  
34 term stability of the growing list of biopharmaceuticals such as antibodies, hormones,  
35 vaccines, therapeutics peptides and proteins. This method makes it possible to remove the  
36 majority of water at temperatures far below 0 °C (usually between -40 °C and -20 °C) by  
37 sublimation, the phase transition from ice to water vapor.<sup>1</sup>

38 Due to the really low temperature and pressure typically used, freeze-drying remains a time  
39 consuming process often difficult to control and scale-up. The US Food and Drug  
40 Administration has recently proposed a new regulatory philosophy to manage product  
41 quality: the Quality by Design (QbD) initiative. Quality will be no more tested into the  
42 product but designed into the process. The QbD approach is based on pre-defined quality  
43 targets and on a deep understanding of how formulations and process interact to influence  
44 critical quality attributes of pharmaceutical products.<sup>2</sup> In contrast to tablets, products intended  
45 to be freeze-dried are conditioned in their final packaging system (vial or syringe) before the  
46 process.<sup>3</sup> The vial thus directly influences the freeze-drying process and impacts final product  
47 quality.<sup>4,5</sup> Furthermore, since the capacity of a manufacturing freeze-dryer can easily reach  
48 100 000 vials, ensuring uniform product quality attributes (potency of the active ingredient,  
49 residual moisture content, visual aspect of the freeze-dried cake) within the entire batch  
50 represents a real challenge. Any variation in the design of the packaging system or other  
51 parameters could result in product quality variation.

52 Product temperature is a key process parameter governing an important critical product  
53 quality attribute, the visual aspect of the freeze-dried cake, which in turn could influence the  
54 residual moisture, the stability of the active ingredient and the reconstitution time.<sup>6</sup> During  
55 the process the product temperature should be maintained below a critical value  
56 corresponding to the glass transition temperature in amorphous product.<sup>3,7</sup> However, the

57 product temperature profile cannot be directly controlled and depends on the process  
58 operating parameters (i.e., shelf temperature, chamber pressure) and on the heat transfer  
59 through the container (e.g., vial).<sup>4,7,8</sup> Knowledge of the heat transfer characteristics of the vial  
60 and the uniformity or non uniformity of this property within vial arrangement inside a freeze-  
61 dryer is thus essential to be able to predict final quality of the product batch. Several authors  
62 have reported that the heat transfer rate between the shelf and the product is dependent on the  
63 vial position on the shelf.<sup>4,5,9-12</sup> Pikal et al.<sup>5</sup> showed that the vials located at the periphery of  
64 the shelf exhibited sublimation rates 15% higher than vials located in the center. This  
65 phenomenon, referred to as "edge effect", has been ascribed to additional heat transfer by  
66 radiation from walls and doors.<sup>4,5,8,9,11</sup> The higher heat flow rate of these periphery vials  
67 could lead to product collapse due to increased product temperatures during the primary  
68 drying phase. Furthermore, Pisano et al.<sup>10</sup> recently observed a normal distribution in the vial  
69 heat transfer coefficient evaluated for vials located in the center of the shelf.

70 The design of the vial also strongly influences the heat transfer efficiency between the shelf  
71 and the product.<sup>4,5,7,12-15</sup> Considering that the vials are placed directly on the shelf, the heat  
72 flow transferred to the product can be described by three parallel mechanisms: conduction  
73 from the shelf surface to the vial *via* points of direct contact between the vial bottom and the  
74 shelf, conduction through the vapor entrapped in the vial bottom concavity and radiation.<sup>5,8,12</sup>  
75 Heat transfers *via* contact conduction and conduction through the gas are influenced,  
76 respectively, by the dimension of the contact area between the shelf and the vial and the  
77 depth of bottom curvature in which the gas is entrapped.<sup>5,8,12</sup> Several studies<sup>13,16,17</sup> have  
78 demonstrated that the vial bottom curvature limits the heat transfer and, thus, the sublimation  
79 flow rate that determines the duration of the primary drying. The concavity of the vial bottom  
80 limits the direct surface contact between the vial and the shelf, accounting for most of the  
81 resistance to conductive heat transfer.<sup>14,16</sup> In pharmaceutical freeze-drying conditions, contact

82 conduction is more efficient than gas conduction, and an increase in the contact area leads to  
83 a significant increase in the total heat transfer.<sup>5,14</sup>

84 Our objective was to quantitatively investigate the role of vial geometry distribution on heat  
85 transfer heterogeneity and subsequently on product quality by predicting product temperature  
86 distribution during the primary drying step induced by variability in vial dimensions.  
87 Proposing an approach to understand how vial design and operating conditions interact to  
88 influence product quality is completely in the scope of the QbD approach.

89 In the present study, only vials located in the center of the shelf and surrounded by other vials  
90 in the same conditions were considered so as to avoid any heterogeneity due to the additional  
91 border heat transfer. The analysis of the heterogeneity was conducted in terms of vial heat  
92 transfer coefficient ( $K_v$ ) distributions. Based on theoretical analysis,<sup>5,8,12</sup> attention was  
93 focused on the role of two vial dimensions, the bottom curvature depth and the contact area  
94 between the bottom vial and the shelf. Two shelf temperatures (-40 °C and 0 °C) and six  
95 chamber pressures (4, 6, 9, 15, 40 and 50 Pa) were tested in two freeze-dryer pilot plants of  
96 similar shelf emissivity to assess the impact of these operative parameters on the heat transfer  
97 heterogeneity among central vials. Finally, as example of practical application of our work  
98 for assessing the pharmaceutical product quality, the impact of the central vial  $K_v$  variability  
99 on product temperature was evaluated. Product temperature distributions for a 5 % sucrose  
100 solution were calculated from the simulated  $K_v$  distributions based on the vial geometry for  
101 several operating conditions.

102

## 103 **MATERIALS AND METHODS**

### 104 **Materials**

105 Siliconized glass tubing vials (3 mL) were provided by Müller + Müller (Holzminden,  
106 Germany). These vials are routinely used in commercial manufacturing. Distilled water was  
107 used throughout the experiments.

108 Two pilot scale freeze-dryers differing mainly by their size, the type of valve connecting the  
109 drying chamber to the condenser and their age were used for this study:

110 - a LyoVac GT6 (Finn-Aqua Santasalo-Sohlberg SPRL, Brussels, Belgium), referred to as  
111 LYO A. It included 5 shelves with an area of 0.14 m<sup>2</sup> each, a distance between shelves of 56  
112 mm, a drying chamber volume of 0.061 m<sup>3</sup> and a butterfly valve between the chamber and  
113 the condenser.

114 - an Epsilon 2-25D (Martin Christ Gefriertrocknungsanlagen GmbH, Osterode am Harz,  
115 Germany), referred to as LYO B. It included 7 shelves with an area of 0.27 m<sup>2</sup> each, a  
116 distance between shelves of 55 mm, a drying chamber volume of 0.38 m<sup>3</sup> and a mushroom  
117 valve between the chamber and the condenser.

118 The pressure in the freeze-dryer chamber was monitored by a capacitive manometer. Since it  
119 was not technically possible to install thermocouples in the drying chamber of the two freeze-  
120 dryers, Tempris wireless sensors (IQ Mobil Solution GmbH, Holzkirchen, Germany) were  
121 positioned in the bottom center of selected vials (Figure 1) to record ice temperature during  
122 the experiments. The obtained signal was used to define the sublimation starting point.

123

#### 124 **Ice sublimation experiments**

125 All experiments were performed using a 1.8 mL fill volume of distilled water (filling height:  
126 11 mm). No stopper was inserted into the vial neck. The middle shelf was fully covered by  
127 filled vials for all runs, corresponding to a total of 540 vials in LYO A and 950 vials in LYO  
128 B. Bottomless trays were used.

129 The vials were quickly loaded on the pre-cooled shelf at -50°C. The presence of a dry laminar  
130 flow in front of the freeze-dryer door made it possible to control the air relative humidity and  
131 thus to limit condensation on the shelves. After a freezing step of 2 hours, the pressure was  
132 decreased and the shelf temperature was increased by 1 °C/min. Experiments were carried out  
133 at 4, 6, 9, 15, 40 and 50 Pa with a shelf fluid inlet temperature of 0 °C, and at 4 and 6 Pa with  
134 a shelf fluid inlet temperature of -40 °C. The run performed at 0 °C and 6 Pa was repeated  
135 three times. The cycles were run long enough to dry up to 20-25 % of the initial fill volume.  
136 Subliming a larger quantity of ice could lead to loss of contact between the vial and the ice,  
137 introducing uncertainty in the analysis.

138 The sublimation rate  $\dot{m}$  was measured gravimetrically for each vial and calculated as the  
139 mass loss divided by the period of sublimation. A total of 100 vials, placed in the centre of  
140 the shelf and surrounded by other vials in the same conditions, were individually weighed  
141 before and after the experiment on a precision scale ( $\pm 0.001$  g; Mettler Toledo, Zaventem,  
142 Belgium). Sublimation time was measured from the moment when shelf temperature  
143 exceeded product temperature, meaning that there was a net heat flux from the shelf towards  
144 the vials. The arrangement of the weighed vials within the shelves is shown in Figure 1 for  
145 the two freeze-dryers.

146

#### 147 **Measurement of emissivity of the vial and of the shelf**

148 Emissivity measurements were performed by Themacs Ingénierie (Champs sur Marne,  
149 France). The glass vial emissivity was determined using a Fourier transform infrared  
150 spectrophotometer (Frontier, Perkin Elmer, Roissy, France) equipped with a Pike<sup>®</sup> integrant  
151 sphere (Pike Technologies, Fitchburg, WI, USA). The measured emissivity varied from 0.78  
152 to 0.80 within the range of temperatures tested (from -48 °C to 27 °C). Thus, a constant value



153 corresponding to the average observed product temperatures (between -48 to -24 °C) was  
154 used in the data analysis, as reported in Table 1.

155 The shelf emissivity was measured using the emissometer EM-2, making it possible an in situ  
156 measurement.<sup>18</sup> The emissivity value of the shelves of LYO B was  $0.18 \pm 0.06$  (Table 1).  
157 Measurements were carried out on several pilot and production freeze-dryers and shelf  
158 emissivity values in the range of 0.18-0.3 were obtained. Considering the relative standard  
159 deviation of the method (0.06), the measured values are in agreement with values reported in  
160 literature.<sup>5</sup>

161

### 162 **Dimensional analysis of a batch of vials**

163 The dimensions of 120 vials were precisely measured by the specialized company  
164 Precis&Mans (Le Mans, France) using the micrometer Mitutoyo 3D (Mitutoyo Europe  
165 GmbH, Neuss, Germany). The following geometrical parameters were determined with a  
166 precision of 0.003 mm: the inner and outer bottom radius and the maximum bottom curvature  
167 depth. These values were used to calculate additional vial dimensions: outer and inner vial  
168 bottom area, vial shelf contact area ( $A_c$ ) (named radius-based contact area in Table 1) and  
169 mean bottom curvature depth ( $l$ ) (Appendix).

170 Furthermore, the vial-shelf contact area was also estimated using the imprint method  
171 proposed by Kuu et al.<sup>17</sup> and Hibler et al.<sup>4</sup> The vials were gently placed on an inkpad and then  
172 on a sheet of white paper. ImageJ v.1.49 software (National Institutes of Health, Bethesda,  
173 MD, USA) was used for the determination of the vial-shelf bottom contact area in pixels from  
174 the imprint images. The scale factor of pixels in  $\text{mm}^2$  was determined by evaluating the  
175 number of pixels of a black shape of known area and was equal to  $0.0153 \text{ mm}^2 \text{ pixel}^{-1}$ . The  
176 mean value and the relative standard deviation of these geometrical dimensions are reported  
177 in Table 1. The two methods used for evaluating the vial-shelf contact area gave similar mean

178 values: 16.7 mm<sup>2</sup> for the imprint method and 17.8 mm<sup>2</sup> for the dimensional analysis.  
179 However, the coefficient of variation of these methods appeared different and significantly  
180 higher for the imprint method (23.9 % versus 12.0 % for the dimensional analysis). The  
181 values of contact area determined using this latter method were selected for the analysis  
182 considering that this method better accounts for intimate contact between vial and shelf.

183

## 184 **THEORY AND DATA ANALYSIS**

### 185 **Evaluation of the vial heat transfer coefficient $K_v$ based on experimental data**

186 As widely reported in literature,<sup>4,5,8,12</sup> the vial heat transfer coefficient  $K_v$  was calculated  
187 using the following equation:

188

$$189 \quad K_v = \frac{\dot{Q}}{A_b(T_s - T_b)} = \frac{\Delta H \dot{m}}{A_b(T_s - T_b)} \quad \text{Equation 1}$$

190

191 where  $\dot{Q}$  is the heat flow received by the vial,  $A_b$  is the outer vial bottom area,  $T_s$  is the  
192 average temperature between the inlet and outlet shelf fluid temperatures,  $T_b$  is the bottom  
193 product temperature,  $\Delta H$  is the latent heat of sublimation and  $\dot{m}$  is the sublimation rate.

194 Since it was not possible to implement thermocouples in the freeze-dryer pilot plant to have a  
195 precise measurement of the product temperature,  $T_b$  was theoretically determined as:

196

$$197 \quad \dot{Q} = \frac{\lambda_{ice}}{L_{ice}} A_{in} (T_b - T_i) \quad \text{Equation 2}$$

198

199 where  $\lambda_{ice}$  is the ice thermal conductivity,  $A_{in}$  is the inner bottom area of the vial,  $L_{ice}$  is the  
200 ice thickness and  $T_i$  is the ice-vapor interface temperature. The ice thickness was estimated as

201 the mean between the initial and final ice thickness values (calculated using the amounts of  
202 initial and sublimed ice).

203 No stopper and pure water were used in this study in order to assume that the partial pressure  
204 of vapor at the sublimation interface was equal to the chamber pressure. The temperature at  
205 the ice-vapor interface  $T_i$  was thus calculated as a function of the interface pressure  $P_i$  using  
206 the Clausius-Clapeyron relation:<sup>19</sup>

207

$$208 \quad T_i = \frac{6139.6}{28.8912 - \ln(P_i)} \quad \text{Equation 3}$$

209

210 The  $T_b$  value calculated was compared to the product temperature value given by the Tempris  
211 probe and an excellent agreement between experimental and theoretical data was observed.

212

### 213 **Theoretical description of the vial heat transfer coefficient $K_v$**

214 The main objective of this work was to quantify the impact of vial dimensions distribution on  
215 heat transfer variability and its resulting consequence on product temperature. To this end,  
216 the vial heat transfer coefficient need to be theoretically expressed in function of specific vial  
217 dimensions.

218 The vial heat transfer coefficient  $K_v$  can be described as the sum of three contributions:<sup>5,8,12</sup>

219

$$220 \quad K_v = K_c + K_g + K_r \quad \text{Equation 4}$$

221

222 where  $K_c$  represents the thermal contact conduction between the shelf and the vial *via* the  
223 direct contact area,  $K_g$  the thermal conduction through the gas entrapped in the vial bottom  
224 curvature and  $K_r$  the thermal radiation between the vial and the top and bottom shelves.

225

226

227 *Heat transfer by thermal contact conduction  $K_c$*

228 The expression of  $K_c$  has been discussed in the literature by only a few authors.<sup>16,17</sup> Kuu et  
229 al.<sup>17</sup> proposed an evaluation of this parameter and showed that the larger the contact area is,  
230 the larger the value of the contact conduction coefficient will be. Thus,  $K_c$  can be assumed to  
231 be proportional to the contact area ( $A_c$ , evaluated by the imprint test method) through an  
232 empirical constant ( $C_1$ ):

233

$$234 \quad K_c = C_1 A_c \quad \text{Equation 5}$$

235

236 *Heat transfer by conduction through the gas  $K_g$*

237 The coefficient  $K_g$ , representing the contribution of the conduction through the gas in  $K_v$ , can  
238 be expressed as:<sup>5,12</sup>

239

$$240 \quad K_g = \frac{C_2 P_C}{1 + \frac{C_2 l}{\lambda_{amb}} P_C} \quad \text{Equation 6}$$

241

242 where  $P_C$  is the chamber pressure,  $\lambda_{amb}$  is the molecular conductivity of the water vapor at  
243 ambient pressure,  $l$  is the mean vial bottom curvature depth calculated as reported in the  
244 Appendix, and the coefficient  $C_2$  is equal to:

245

$$246 \quad C_2 = \Lambda_o \frac{\alpha_c}{2 - \alpha_c} \left( \frac{273.15}{T_{gas}} \right)^{0.5} \quad \text{Equation 7}$$

247

248 where  $\Lambda_o$  is the free molecular heat conductivity of the gas at 0 °C,  $T_{gas}$  is temperature of the  
249 gas participating to heat conduction, calculated as average between the product temperature

250 at the sublimation interface and the shelf temperature values,<sup>12</sup> and  $\alpha_c$  is the accommodation  
251 coefficient.

252 *Heat transfer by thermal radiation  $K_r$*

253 The heat transfer by radiation between the shelf and the vial  $\dot{Q}_r^{shelf}$  can be described by the  
254 Stephen-Boltzmann equation:<sup>5,8,20</sup>

255

$$256 \quad \dot{Q}_r^{shelf} = A_r \mathcal{F} \sigma (T_s^4 - T_b^4) \quad \text{Equation 8}$$

257

258 where  $A_r$  is the area exposed to the radiation from the shelves to be considered equal to the  
259 vial bottom area  $A_b$ ,  $\mathcal{F}$  is the visualization factor and  $\sigma$  the Stephan-Boltzman constant. After  
260 mathematical rearrangement, Equation 8 can be expressed as:

261

$$262 \quad \dot{Q}_r^{shelf} = A_r \mathcal{F} \sigma (T_s^4 - T_b^4) = A_b \mathcal{F} \sigma (T_s + T_b)(T_s^2 + T_b^2)(T_s - T_b) \quad \text{Equation 9}$$

263

264 Thus, the heat transfer coefficient  $K_r$  for thermal radiation can be defined as:

265

$$266 \quad K_r = \mathcal{F} \sigma (T_s + T_b)(T_s^2 + T_b^2) \quad \text{Equation 10}$$

267

268 During the process, central vials are affected by two different radiative heat transfer  
269 contributions: between (i) the shelf below the vial and the vial bottom, and (ii) the shelf  
270 above the vial and the top of the vial.<sup>5,8,12</sup> Hence, the visualization factor will be the sum of  
271 two terms:

272

$$273 \quad \mathcal{F} = \mathcal{F}_b + \mathcal{F}_{top} \quad \text{Equation 11}$$

274

275 The visualization factor at the bottom of the vial  $\mathcal{F}_b$  can be evaluated considering the  
 276 definition proposed by Bird et al.<sup>20</sup> and Pikal<sup>8</sup> for the heat transfer by radiation between  
 277 parallel surfaces:

278

$$279 \quad \mathcal{F}_b = \frac{1}{1 + \left(\frac{1}{e_v} - 1\right) + \left(\frac{1}{e_s} - 1\right)} \quad \text{Equation 12}$$

280

281 where  $e_v$  and  $e_s$  are the emissivities of the vial and shelf, respectively.

282 Considering vials located in the centre of the shelf and surrounded by other vials in the same  
 283 conditions, it is possible to assume that (i) the vial area exposed to the top shelf is much  
 284 smaller than the area of the shelf and (ii) the vial top does not receive radiations from the side  
 285 walls of the chamber. Thus, the visualization factor between the top of the vials and the shelf  
 286  $\mathcal{F}_{top}$  can be estimated equal to the emissivity of the vial:<sup>5,8</sup>

287

$$288 \quad \mathcal{F}_{top} = e_v \quad \text{Equation 13}$$

289

290 In agreement with the literature, the visualization factor at the vial top (equal to 0.78; Table  
 291 1) is higher than the one at the vial bottom (equal to 0.16; Table 1).<sup>5</sup>

292

293 *Dependence of the vial heat transfer coefficient on vial geometry*

294 Equations 4, 5 and 6 were combined to highlight the dependence of  $K_v$  on the contact area  
 295 ( $A_c$ ), and bottom curvature depth ( $l$ ):

296

$$297 \quad K_v = C_1 A_c + K_r + \frac{C_2 P_c}{1 + \frac{l}{\lambda_{amb}} C_2 P_c} \quad \text{Equation 14}$$

298

299 The term  $K_r$  was calculated from Equations 10-13 for each experimental condition.  
300 Coefficients  $C_1$  and  $C_2$  were determined by fitting Equation 14 in a least-squares sense to  
301 experimental  $K_v$  values determined by the gravimetric method. Calculations were performed  
302 with Matlab R2014b software equipped with the Statistics Toolbox (The Mathworks Inc.,  
303 Natick, MA, USA). The bottom curvature depth  $l$  and contact area  $A_c$  were evaluated from  
304 dimensional analysis of the vial and imprint test, respectively.

305

### 306 **Calculation of $K_v$ distributions based on vial geometry**

307 Two vial dimensions influence heat transfer: the contact area ( $A_c$ ) and the mean bottom  
308 curvature depth ( $l$ ). The absence of correlation between the two geometrical dimensions  $l$  and  
309  $A_c$  was verified by calculating the correlation factor together with its statistical significance  
310 (p-value > 0.5). It was thus possible to independently evaluate the impact of those parameters  
311 on  $K_v$ . Using Equation 14, three  $K_v$  distributions based on vial dimension variations were  
312 simulated: (i) curvature-based ( $l$  in Equation 14); (ii) contact area-based ( $A_c$  in Equation 14);  
313 and (iii) their combination. The curvature-based  $K_v$  distribution was obtained by evaluating  
314 Equation 14 with the 120 measured values of the mean bottom curvature depth ( $l$ ), while the  
315 contact area was maintained constant at its mean value. The contact area-based  $K_v$   
316 distribution was obtained by evaluating Equation 14 with the 120 measured values of the  
317 imprint-based contact area ( $A_c$ ), whereas the bottom curvature depth was maintained constant  
318 at its mean value. Plugging both measured  $l$  and  $A_c$  values into Equation 14 gave the  
319 combined contact area and curvature-based  $K_v$  distribution. The calculation was repeated for  
320 all the studied chamber pressures and shelf temperatures. Chi-square goodness-of-fit tests were  
321 performed on the simulated  $K_v$  distributions, establishing that the sample data were consistent  
322 with a normal distribution at a 0.05 significance level.

323

## 324 **Simulation of the product temperature distributions using the $K_v$ distribution**

325 Product temperature distributions were obtained from the calculated contact area and  
326 curvature-based  $K_v$  distribution. The product temperature was calculated for a 5 % w/w  
327 sucrose solution, considering a shelf temperature of -25°C and four chamber pressures (4, 6,  
328 9, 15 Pa). Pressure at 40 and 50 Pa were not considered because the product temperature  
329 exceeds the glass transition temperature of the product at such high pressure (i.e., -32 °C for a  
330 5 % w/w sucrose solution).<sup>21</sup> In the case of a real product, the mass flow rate can be  
331 expressed as reported by Pikal et al.<sup>5</sup>:

332

$$333 \quad \dot{m} = \frac{(P_t - P_c) A_{in}}{R_p} \quad \text{Equation 15}$$

334

335 where  $R_p$  represents the area-normalized product resistance. The value of  $R_p$  used for this  
336 simulation is reported in Table 1 and was considered for a dried layer thickness of 0.5 cm.<sup>21</sup>  
337 To simulate the product temperature distribution, the non-linear system composed of  
338 Equations 1-3 and 14-15 was solved for each pair of measured  $l$  and  $A_c$  values. Chi-square  
339 goodness-of-fit tests were performed on the product temperature distributions, demonstrating  
340 that the simulated data were compatible with a normal distribution at a 0.05 significance  
341 level.

342

## 343 **RESULTS AND DISCUSSION**

### 344 **Impact of equipment on $K_v$**

345 Vial heat transfer coefficient  $K_v$  of 100 vials located in the centre of the shelf was  
346 experimentally determined for different chamber pressures (4 to 50 Pa), shelf temperatures (-  
347 40 °C and 0 °C) and freeze-dryers (LYO A and LYO B). Figure 2 illustrates the evolution of  
348 the average value of  $K_v$  with pressure. Equation 14 was fitted with the experimental data and



349 the resulting coefficients  $C_1$  and  $C_2$  are presented in Table 2 for the data obtained in LYO A,  
350 LYO B and their combination. The accommodation coefficient  $\alpha_c$  was also calculated from  
351 Equation 7, considering an average value of the gas temperature obtained under the different  
352 operating conditions tested ( $T_{gas} = -35$  °C). The obtained values of the accommodation  
353 coefficient appear to be in agreement with data in literature.<sup>8</sup>

354 In Table 2, LYO A and LYO B exhibited a similar value of the  $C_1$  coefficient that is related  
355 to the contact area coefficient  $K_c$  (Equation 5), but distinct values of the  $C_2$  coefficient that is  
356 related to  $K_g$  (Equation 6). LYO B exhibited a slightly higher accommodation coefficient  
357 than LYO A, probably due to a different finish of the freeze-dryer shelf material.

358 When considering pressure values lower than 10 Pa (Figure 2), the  $K_v$  values obtained in the  
359 two freeze-dryer appeared similar. This result was confirmed also by Pisano,<sup>12</sup> who reported  
360 no significant difference in  $K_v$  value of central vials processed in a pilot and manufacturing  
361 freeze-dryer at a pressure of 10 Pa. For pressure value higher than 10 Pa, the influence of  
362 freeze-dryer configuration became significant with slightly higher values obtained in LYO B  
363 (Figure 2). At 50 Pa, the  $K_v$  value was approximately 8% higher in LYO B than in LYO A.  
364 Considering the different values of  $C_2$  coefficient, the  $K_v$  difference between freeze-dryers at  
365 high pressure can thus be ascribed to the increased rate of heat transfer through the gas over  
366 the total heat flow. However, the physical origin of the differences in the pressure-dependent  
367 component of  $K_v$  remains unclear. Possible hypotheses include: (i) differences in the shelf  
368 surface finish that could induce differences in the gas-shelf heat transfer through the  
369 accommodation coefficient<sup>8</sup> (Equation 6-7) as well as (ii) differences in the gas convection  
370 conditions, a mechanism responsible for a small part of the pressure-dependent heat  
371 transfer.<sup>22</sup> These results suggest that small differences between devices might become more  
372 apparent at high pressures. When considering only vials not exposed to edge effect a cycle  
373 designed with low operating pressure (below 10 Pa) could therefore be more suitable for safe

374 scale-up. However the behavior of the edge vials located at the periphery of the shelf or in  
375 contact with metallic band need also to be considered and some elements were recently  
376 proposed by Pikal et al.<sup>11</sup> to investigate the impact of the freeze-dryer configuration.

377

### 378 **Impact of chamber pressure and shelf temperature on $K_v$**

379 As reported in the literature and shown in Figure 2, chamber pressure had a strong impact on  
380  $K_v$ .<sup>4,5,8,12,13,15</sup> The vial heat transfer coefficient increased approximately four times between 4  
381 and 50 Pa. At the vial bottom, the presence of the curvature limits the intimate contact  
382 between the shelf and the vial and create an empty space between the shelf and the vial that  
383 acts as an insulator.<sup>13,16,17</sup> At very low pressures typically used in the process, the heat  
384 transfer contribution by gas convection is usually neglected,<sup>11</sup> whereas the contribution of gas  
385 conduction has to be considered. This heat transfer mechanism, represented by the coefficient  
386  $K_g$ , is dependent on the chamber pressure and increases when increasing pressure, as shown  
387 in Equation 6.<sup>5,8,12,15</sup> Figure 3 shows the relative contributions of  $K_c$ ,  $K_r$  and  $K_g$  on the total  
388  $K_v$ , calculated using the set C of the fitting coefficients reported in Table 2. The  $K_c$  and  $K_r$   
389 contributions go from about 30 % at 4 Pa to 10 % at 50 Pa, whereas the  $K_g$  contribution goes  
390 from about 25 % at 4 Pa to 80 % at 50 Pa.

391 A moderate effect of shelf temperature on  $K_v$  was expected theoretically due to  $K_r$  (Equation  
392 10) and to  $K_g$  through the gas temperature (Equations 6-7). Figure 4a displays the influence  
393 of shelf temperature on  $K_v$ . Differences in  $K_v$  values due to temperature remained within the  
394 standard deviation when considering pressure values lower than 10 Pa and when the  
395 contribution of  $K_g$  in the total  $K_v$  is moderate (around 25 %, Figure 3).

396 In order to clarify the impact of the shelf temperature, the contributions of the single  
397 coefficients  $K_c$ ,  $K_r$  and  $K_g$  on  $K_v$  were calculated for two shelf temperatures (25 °C and -25  
398 °C) and three chamber pressures (4, 6 and 50 Pa), as show in Figure 4b. The contact

399 conduction coefficient  $K_c$  does not depend on the shelf temperature (Equation 5) and thus has  
400 a constant contribution in  $K_v$  for all the temperatures tested. The radiative coefficient  $K_r$   
401 depends on the third power of the shelf temperature and increases by about  $1 \text{ W m}^{-2} \text{ K}^{-1}$   
402 between  $-25 \text{ }^\circ\text{C}$  and  $25 \text{ }^\circ\text{C}$  for all pressures considered. The gas conduction coefficient  $K_g$   
403 depends on the gas temperature and decreases by  $0.1\text{-}0.2 \text{ W m}^{-2} \text{ K}^{-1}$  at low pressures (4-6  
404 Pa) and by  $1.1 \text{ W m}^{-2} \text{ K}^{-1}$  at 50 Pa, between the two considered values of shelf temperature.  
405 When increasing shelf temperature, the increase of  $K_r$  is partly compensated by the decrease  
406 of  $K_g$ . These results confirm that the dependence of  $K_v$  on the shelf temperature is negligible,  
407 especially if compared with the role played by the chamber pressure. Pisano et al.<sup>12</sup> and  
408 Hottot et al.<sup>23</sup> reported similar  $K_v$  values for different shelf temperature conditions.

409

#### 410 **Inter-vial heat transfer heterogeneity and the role of vial dimensions**

411 Figure 5 presents the experimentally observed distributions of the vial heat transfer  
412 coefficient data of central vials at six chamber pressures. Since temperature- and equipment-  
413 induced variations were minor, data obtained in LYO A and B and for the two shelf  
414 temperatures were merged. A significant variability in the  $K_v$  values evaluated for central  
415 vials was observed, the standard deviation increasing with pressure from 0.84 to  
416  $2.46 \text{ W m}^{-2} \text{ K}^{-1}$ . The values of standard deviation corresponded to coefficient of variation  
417 comprised between 4 and 8 % depending on the operating conditions. The measurement error  
418 associated to the determination of  $K_v$  was evaluated as the sum of the individual  
419 measurement accuracy of each parameter entering in the calculation of  $K_v$  (Equation 1). The  
420 measurement uncertainty was estimated to be  $\sim 1 \%$ . This value is in agreement with the  
421 value reported by Pikal et al.<sup>5</sup>, who reported an uncertainty value of  $\sim 1.2 \%$ . The  
422 measurement uncertainty alone did not allow to completely explain the variability of the  $K_v$

423 data. An external factor responsible for inter-vial heat transfer heterogeneity had thus to be  
424 considered.

425 Attention was focused on the container: the geometrical difference among the vials was  
426 considered as a possible source of the heat transfer heterogeneity. This variability in the vial  
427 dimensions can be due to production limits and could change as a function of the container  
428 model and provider. For the tested vial set, the coefficient of variation was approximately  
429 27.7 % for the mean bottom curvature depth ( $l$ ) and 23.9 % for the imprint-based contact area  
430 ( $A_c$ ). Hence, the effect of the variability of these geometrical dimensions on  $K_v$  was evaluated  
431 as proposed in the Theory and data analysis section using the set of coefficients C reported in  
432 Table 2.

433 Figure 6 displays the simulated distributions of  $K_v$  based on the vial bottom dimensions.  
434 These distributions showed a trend and range of  $K_v$  values similar to the experimental ones.  
435 At low pressure,  $K_v$  variability is almost completely due to the contact area variability. The  
436 importance of the contact area on the  $K_v$  value was also confirmed by Pikal et al.<sup>5</sup> and  
437 Cannon et al.<sup>16</sup> Regarding the vial bottom curvature, the importance of its variability  
438 increased when the pressure rose. This is due to the coefficient  $K_g$  that plays a major role in  
439 the total value of  $K_v$  at 40 and 50 Pa, as shown in Figure 3. The role of the bottom curvature  
440 dimension was previously investigated by Brülls and Radsmuson<sup>15</sup> and Cannon et al.<sup>16</sup> Brülls  
441 and Radsmuson<sup>15</sup> have shown that the bottom curvature has an impact on the heat transfer  
442 only at chamber pressures higher than 30 Pa. This conclusion was confirmed by Cannon et  
443 al.<sup>16</sup>, who found that bottom curvature had little impact when considering low pressure (< 27  
444 Pa). Our results agree with these conclusions,<sup>15,16</sup> confirming that the variability of the  
445 bottom curvature depth has to be taken into consideration only if cycles at high chamber  
446 pressure are performed (> 30 Pa).

447 Figure 7 displays the coefficient of variation of the experimental and calculated  
448  $K_v$  distributions at different pressures. For the experimental distributions, the coefficient was  
449 calculated as an average between the LYO A and B datasets. The trend of the observed  
450 coefficient of variations for both experimental and simulated  $K_v$  distributions decreased from  
451 approximately 9 % to 4 % when increasing the chamber pressure. The variability of the  
452 experimental  $K_v$  distributions is completely explained by the geometrical variability at low  
453 pressures (i.e., 4, 6 Pa), whereas at higher pressures, the experimental coefficient of variation  
454 appears to be slightly higher than the one calculated based on vial geometry. It is thus  
455 possible that other sources of variability should be taken into consideration, for example  
456 convection in the drying chamber could play a role if higher pressures are considered.<sup>22</sup>  
457 These considerations can guide the selection of the container as a function of the variability  
458 of the vial dimensions. The results obtained show that at low chamber pressure (i.e., 4, 6, 9,  
459 15 Pa), it is important to assess the variability of the contact area between the vial and the  
460 shelf, whereas for cycles performed at high pressure (i.e., 40, 50 Pa), the variability of the  
461 bottom curvature depth becomes a relevant parameter. Consequently, for pharmaceutical  
462 processes that are usually carried out at pressures lower than 10 Pa, the contact area needs to  
463 be taken into account more than the bottom curvature depth.

464

465 **Impact of  $K_v$  heterogeneity on the product temperature distribution within a batch of**  
466 **vials located in the centre of the shelf and not exposed to edge effect**

467 In the case of freeze-drying, product temperature is one of the most important critical quality  
468 parameters. During the process, product temperature must be maintained close to a limit  
469 value (i.e., glass transition temperature for amorphous products,  $T_g$ ) in order to optimize the  
470 process time but not to exceed it so as to guarantee the visual aspect of the cake and the  
471 product quality.

472 The vial-to-vial heat and mass transfer heterogeneity during the sublimation step causes  
473 variability in the product temperature. Considering a constant and fixed value of mass  
474 transfer resistance, it would be interesting to estimate the product temperature distribution  
475 during the primary drying step resulting only from the variability in vial geometry. Product  
476 temperature distributions were thus evaluated considering the contact area and curvature-  
477 based  $K_v$  distributions. For this analysis, a 5 % w/w sucrose solution was considered,  
478 processed at -25 °C and four different pressures (4, 6, 9 and 15 Pa). Relevant data concerning  
479 product resistance and glass transition temperature (-32 °C) were found in the literature.<sup>21</sup> As  
480 expected, product temperature increased from 4 Pa to 15 Pa because of the higher value of  
481 the vial heat transfer coefficient and higher ice sublimation temperature.

482 The variability of the product temperature was estimated to be approximately 0.9 °C at 15 Pa  
483 and as large as 2.2 °C at 4 Pa, considering  $\pm 3$  times the standard deviation that includes 99 %  
484 of the vials (Figure 8). A practical implication of these results is that, at the low pressures  
485 commonly encountered in vaccine freeze-drying, a temperature safety margin of  
486 approximately 2 °C has to be considered with respect to cycles designed on the basis of an  
487 average  $K_v$  value and to vials not exposed to edge effect.

488 Vials located at the periphery of the shelf (i.e., edge vials) receive additional heating due to  
489 the radiation from the chamber walls and the contact with the metallic guardrail. Thus, edge  
490 vials present a higher sublimation rate and a higher product temperature respect central vials.<sup>5</sup>  
491 Tang et al.<sup>24</sup> reports that the temperature difference between edge vials and central vial can be  
492 up to 2 °C at a shelf temperature of 20 °C and up to 4 °C at -30 °C for a chamber pressure of  
493 about 10 Pa. Depending on the operating conditions of the process, the safety product  
494 temperature margin resulting from variability in vial dimensions could be in the same order  
495 of magnitude than the safety margin imposed by the "edge effect".

496

497 **CONCLUSIONS**

498 Implementation of the Quality by Design initiative require a precise definition of the  
499 acceptable range for all product and process variables ensuring the fulfillment of the critical  
500 quality attributes of the final product. The impact of any variation of these variables on the  
501 final quality need to be quantified in advance. In this work, the effect of the variability of  
502 geometrical dimensions observed within a batch of vials (i.e., contact area between the shelf  
503 and the vial and the mean bottom curvature depth) on product quality was explored. The  
504 product quality was evaluating by predicting the product temperature knowing the vial heat  
505 transfer coefficient  $K_v$ . An original approach was proposed to calculate  $K_v$  distribution based  
506 on geometrical dimensions when considering a batch of vials located in the center of the shelf  
507 not exposed to any edge effect. The impact of freeze-dryer configuration and operating  
508 conditions was also considered. When considering low pressure ( $< 10$  Pa), commonly used  
509 for freeze-drying biopharmaceuticals, the influence of freeze-dryer configuration and shelf  
510 temperature on heat transfer characteristics can be neglected and  $K_v$  distribution is  
511 completely explained by the contact area distribution. Furthermore the variability of vial  
512 dimension results in the definition of a product temperature safety margin of 2 °C. However,  
513 additional sources of variability need to be included in QbD approach. In particular, a study  
514 focused on the variability between edge and central vials and its role in cycle scale-up is  
515 presently ongoing.

516

517 **ACKNOWLEDGMENTS**

518 The authors would like to thank Benoit Moreau and Yves Mayeresse (GSK Vaccines) for  
519 reviewing this manuscript and Vincent Ronsse (technician) and Alain Philippart (operator)  
520 (GSK Vaccines) for their help in the data acquisition.

521

522 **CONFLICT OF INTEREST**

523 Erwan Bourlés is an employee of the GSK group of companies. Bernadette Scutellà  
524 participated in a postgraduate PhD program at GSK Vaccines. Stephanie Passot, Fernanda  
525 Fonseca and Ioan Cristian Trelea report no financial conflicts of interest.

526 **FUNDING**

527 This work was funded by GlaxoSmithKline Biologicals S.A., under a Cooperative Research  
528 and Development Agreement with INRA (Institut National de la Recherche Agronomique)  
529 via the intermediary of the UMR (Unité Mixte de Recherche) GMPA (Génie et  
530 Microbiologie des Procédés Alimentaires) at the INRA Versailles-Grignon research center.

531

532 **AUTHORS' CONTRIBUTIONS**

533 Bernadette Scutellà, Stephanie Passot, Erwan Bourlés, Fernanda Fonseca and Ioan Cristian  
534 Trelea were involved in the conception and design of the study. Bernadette Scutellà and  
535 Erwan Bourlés acquired the data. Bernadette Scutellà, Stephanie Passot, Erwan Bourlés,  
536 Fernanda Fonseca and Ioan Cristian Trelea analyzed and interpreted the results. All authors  
537 were involved in drafting the manuscript or revising it critically for important intellectual  
538 content. All authors had full access to the data and approved the manuscript before it was  
539 submitted by the corresponding author.

540



541

## APPENDIX

542 The evaluation of the mean bottom curvature depth  $l$  was performed from geometrical  
543 considerations on the semi-spherical calotte at the vial bottom, as represented in Figure A.

544 The bottom curvature depth depends on the radius of the vial bottom as follows:

545

$$546 \quad l(r) = R_c - a(r) \quad \text{Equation A1}$$

547

548 where  $R_c$  is the radius of the calotte and  $a(r)$  is the distance between the shelf and the vial  
549 bottom, measured normal to the vial bottom:

550

$$551 \quad a(r) = \sqrt{(R_c - l_{max})^2 + r^2} \quad \text{Equation A2}$$

552

553  $R_c$  can be calculated as a function of the maximum bottom curvature depth  $l_{max}$  and the inner  
554 vial bottom radius  $R_i$ :

555

$$556 \quad R_c^2 = R_i^2 + (R_c - l_{max})^2 \quad \text{Equation A3}$$

557

558 The area-mean bottom curvature depth can be defined as the integral of  $l(r)$  on the calotte,  
559 divided by the area:

560

$$561 \quad l = \frac{1}{A} \int l(r) dA \quad \text{Equation A4}$$

562

563 The relevant area for heat transfer by gas conduction is:

564

$$565 \quad A = \pi R_i^2 \quad \text{Equation A5}$$

566

567 and the area element:

568

569

$$dA = 2\pi r dr \quad \text{Equation A6}$$

570

571 Combining Equations A1-A6,  $l$  was calculated as:

572

573

$$l = \frac{2}{R_i^2} \int_0^{R_i} (R_c - \sqrt{(R_c - l_{max})^2 + r^2}) r dr \quad \text{Equation A7}$$

574

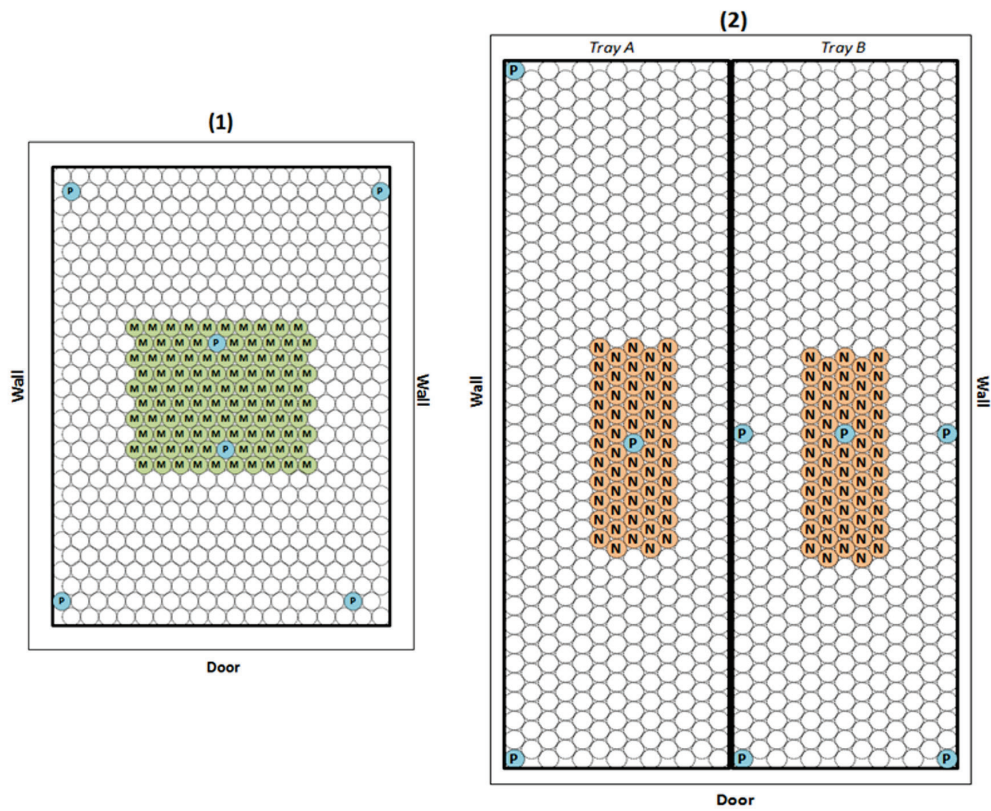
575

576 **REFERENCES**

- 577 1. Jennings TA. 1999. Lyophilization: introduction and basic principles. Englewood, CO:  
578 Interpharm Press.
- 579 2. Nail SL, Searles JA. 2008. Elements of quality by design in development and scale-up of  
580 freeze parenterals. *Biopharm Int* 21(1):44–52.
- 581 3. Franks F. 1998. Freeze-drying of bioproducts: putting principles into practice. *Eur J*  
582 *Pharm Biopharm* 45:221–229.
- 583 4. Hibler S, Wagner C, Gieseler H. 2012. Vial Freeze-Drying, part 1: New Insights into  
584 Heat Transfer Characteristics of Tubing and Molded Vials. *J Pharm Sci* 101(3):1189–  
585 1201.
- 586 5. Pikal MJ, Roy ML, Shah S. 1984. Mass and heat transfer in vial freeze-drying of  
587 pharmaceuticals: role of the vial. *J Pharm Sci* 73(9):1224–1237.
- 588 6. Johnson R, Lewis L. 2011. Freeze-drying protein formulations above their collapse  
589 temperatures: possible issues and concerns. *Am Pharm Rev* 14(3):50–54.
- 590 7. Hibler S, Gieseler H. 2012. Heat transfer characteristics of current primary packaging  
591 systems for pharmaceutical freeze-drying. *J Pharm Sci* 101(11):4025–4031.
- 592 8. Pikal MJ. 2000. Heat and mass transfer in low pressure gases: applications to freeze  
593 drying. In *Drugs and the Pharmaceutical Sciences* 102:611–686.
- 594 9. Rambhatla S, Pikal MJ. 2003. Heat and mass transfer scale-up issues during freeze-  
595 drying, I: atypical radiation and the edge vial effect. *Aaps Pharmscitech* 4(2):22–31.
- 596 10. Pisano R, Fissore D, Barresi AA, Brayard P, Chouvenc P, Woinet B. 2013. Quality by  
597 design: optimization of a freeze-drying cycle via design space in case of heterogeneous  
598 drying behavior and influence of the freezing protocol. *Pharm Dev Technol* 18(1):280–  
599 295.

- 600 11. Pikal MJ, Bogner R, Mudhivarthi V, Sharma P, Sane P. 2016. Freeze-Drying Process  
601 Development and Scale-Up: Scale-Up of Edge Vial Versus Center Vial Heat Transfer  
602 Coefficients, K<sub>v</sub>. *J Pharm Sci* doi:10.1016/j.xphs.2016.07.027.
- 603 12. Pisano R, Fissore D, Barresi AA. 2011. Heat Transfer in Freeze-Drying Apparatus. In:  
604 Dos Santos Bernardes MA ed., *Developments in Heat Transfer* 91-114. Rijeka, Croatia:  
605 InTech. Available from: [http://www.intechopen.com/books/developments-in-heat-](http://www.intechopen.com/books/developments-in-heat-transfer/heat-transfer-infreeze-drying-apparatus)  
606 [transfer/heat-transfer-infreeze-drying-apparatus](http://www.intechopen.com/books/developments-in-heat-transfer/heat-transfer-infreeze-drying-apparatus).
- 607 13. Nail SL. 1980. The Effect of Chamber Pressure on Heat Transfer in the Freeze Drying of  
608 Parenteral Solutions. *PDA J Pharm Sci Technol* 34(5):358–368.
- 609 14. Ybema H, Kolkman-Roodbeen L, te Booy MP, Vromans H. 1995. Vial lyophilization:  
610 calculations on rate limitation during primary drying. *Pharm Res* 12(9):1260–1263.
- 611 15. Brülls M, Rasmuson A. 2002. Heat transfer in vial lyophilization. *Int J Pharm* 246(1-  
612 2):1–16.
- 613 16. Cannon A, Shemeley K. 2004. Statistical evaluation of vial design features that influence  
614 sublimation rates during primary drying. *Pharm Res* 21(3):536–542.
- 615 17. Kuu WY, Nail SL, Sacha G. 2009. Rapid determination of vial heat transfer parameters  
616 using tunable diode laser absorption spectroscopy (TDLAS) in response to step-changes  
617 in pressure set-point during freeze-drying. *J Pharm Sci* 98(3):1136–1154.
- 618 18. Monchau JP, Marchetti M, Ibos L, Dumoulin J, Feuillet V, Candau Y. 2014. Infrared  
619 Emissivity Measurements of Building and Civil Engineering Materials: A New Device  
620 for Measuring Emissivity. *Int J Thermophys* 35:1817-31.
- 621 19. Trelea IC, Passot S, Fonseca F, Marin M. 2007. An Interactive Tool for the Optimization  
622 of Freeze-Drying Cycles Based on Quality Criteria. *Dry Technol* 25(5):741–751.
- 623 20. Bird RB, Stewart WE, Lightfoot EN. 1960. *Transport phenomena*. New York, NY: John  
624 Wiley & Sons.

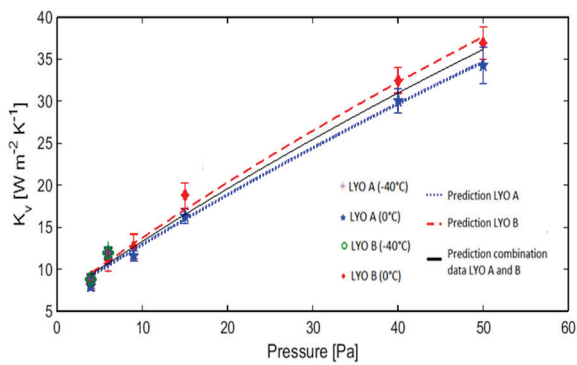
- 625 21. Konstantinidis AK, Kuu W, Otten L, Nail SL, Sever RR. 2011. Controlled nucleation in  
626 freeze -drying: Effect  
627 and primary drying rate. *J Pharm Sci* 100(8):3453–3470.
- 628 22. Ganguly A, Nail SL, Alexeenko A. 2013. Experimental Determination of the Key Heat  
629 Transfer Mechanisms in Pharmaceutical Freeze-Drying. *J Pharm Sci* 102(5):1610–1625.
- 630 23. Hottot A, Vessot S, Andrieu J. 2005. Determination of mass and heat transfer parameters  
631 during freeze-drying cycles of pharmaceutical products. *PDA J Pharm Sci Technol* 59(2):  
632 138–153.
- 633 24. Tang X, Nail SL, Pikal MJ. 2006. Evaluation of manometric temperature measurement, a  
634 process analytical technology tool for freeze-drying: Part I, product temperature  
635 measurement. *AAPS PharmSciTech* 7(1):E95–E103.
- 636
- 637



639

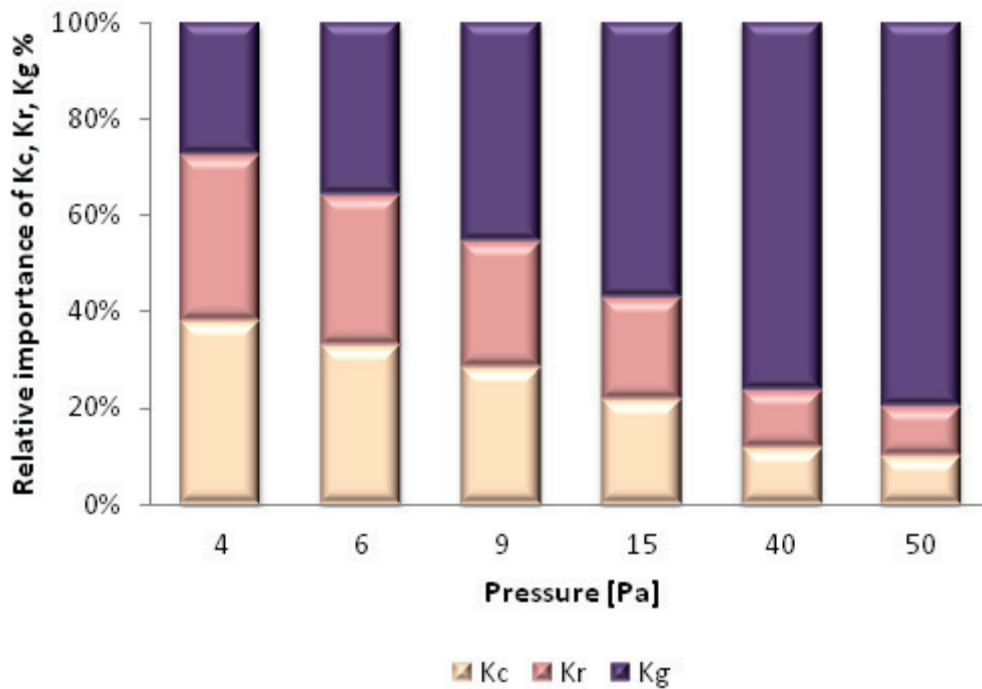
640 **Figure 1.** Vial arrangements in (1) LYO A and (2) LYO B. Gravimetrically-analyzed vials  
 641 are marked with the letters M and N for LYO A and B, respectively. Vials in which wireless  
 642 temperature probes were located are marked with the letter P. All vials were filled with 1.8  
 643 mL of pure water.

644

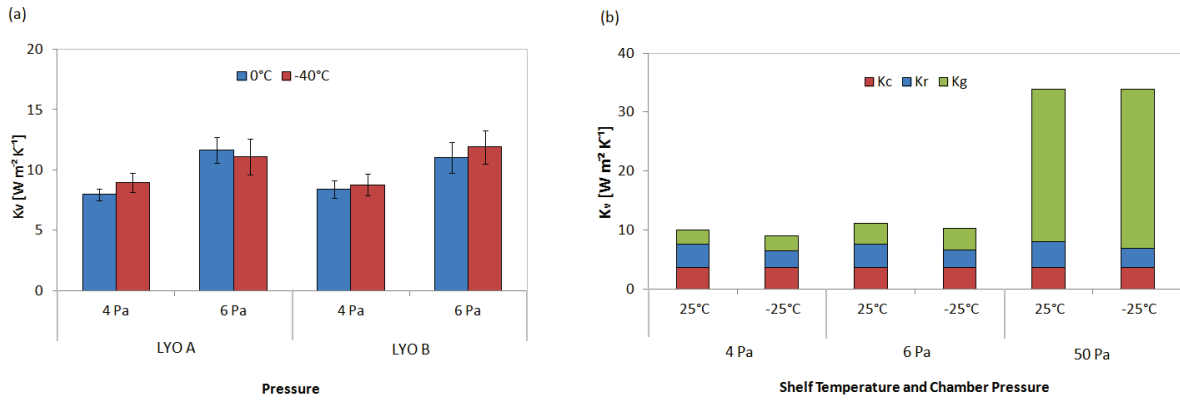


645

646 **Figure 2.** Vial heat transfer coefficient ( $K_v$ ) values vs. chamber pressure ( $P_c$ ). The markers  
 647 refer to the  $K_v$  average values measured in LYO A and B at  $-40^\circ\text{C}$  and  $0^\circ\text{C}$ . The lines  
 648 correspond to the values calculated with Equation 14 with the data obtained from LYO A, B  
 649 and their combination. Error bars represent standard deviations.  
 650



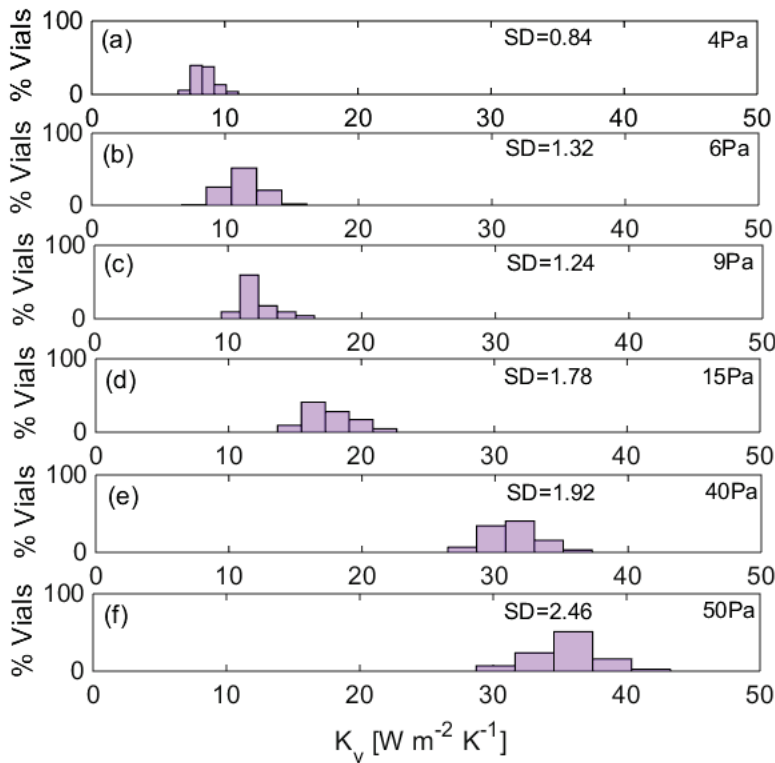
651  
 652 **Figure 3.** Relative importance of the heat transfer coefficients by contact conduction ( $K_c$ ),  
 653 radiation ( $K_r$ ) and conduction through the gas ( $K_g$ ) as percentages of the total heat transfer  
 654 coefficients ( $K_v$ ). Average values of the contact area ( $A_c$ ) and mean bottom curvature depth  
 655 ( $l$ ) were considered in this calculation. The set of coefficients C (Table 2) was used to  
 656 evaluate  $K_c$  and  $K_g$ .  
 657



658

659 **Figure 4.** Influence of the shelf temperature on the vial heat transfer coefficients  $K_v$ .  $K_v$   
 660 values were evaluated at different shelf temperatures and chamber pressures (a) from  
 661 experimental data obtained in LYO A and B and (b) from the coefficients  $K_c$ ,  $K_r$  and  $K_g$ ,  
 662 calculated using Equations 5, 6 and 10.

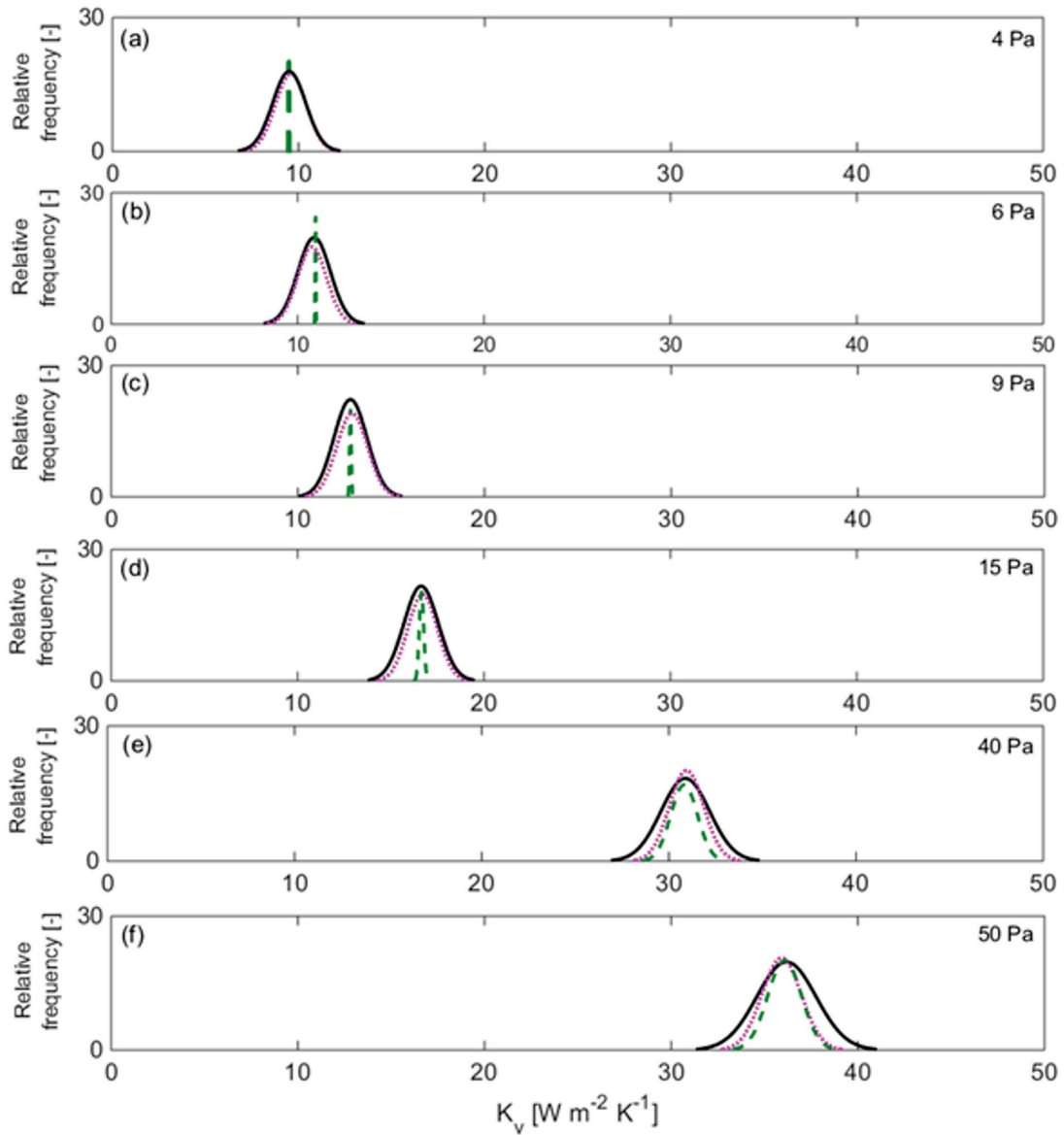
663



664

665 **Figure 5.** Experimentally-measured distribution of the vial heat transfer coefficients at 4 Pa  
 666 (a), 6 Pa (b), 9 Pa (c), 15 Pa (d), 40 Pa (e) and 50 Pa (f). Data of LYO A and LYO B at  
 667 different shelf temperatures (0°C and -40°C) were combined.





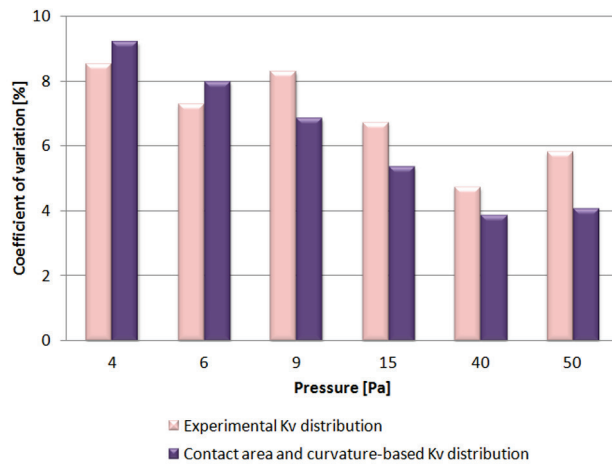
669

670 **Figure 6.** Calculated  $K_v$  normal distributions: curvature-based (dashed green line - -),

671 contact area-based (dotted red line - - -) and combined curvature and contact area-based

672 (solid black line —) at 4 Pa (a), 6 Pa (b), (c) 9 Pa (c), 15 Pa (d), 40 Pa (e) and 50 Pa (f).

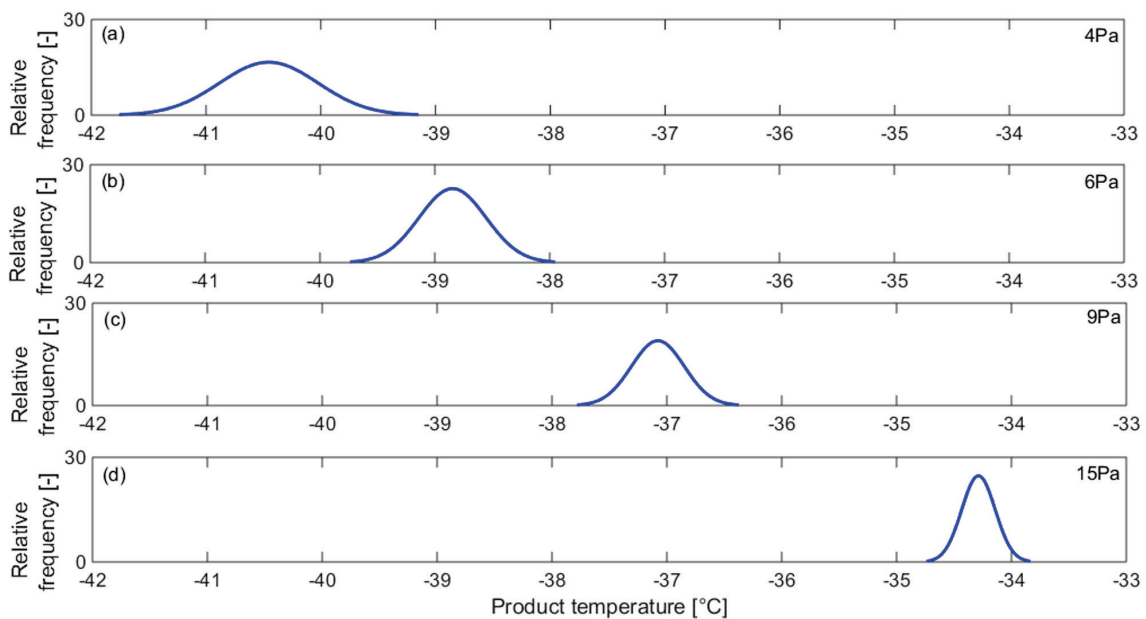
673



674

675 **Figure 7.** Coefficients of variation of experimentally-measured  $K_v$  distribution (LYO A and  
 676 B; light bars) and calculated (combined contact area and curvature-based)  $K_v$  distribution  
 677 (dark bars) and at different pressures.

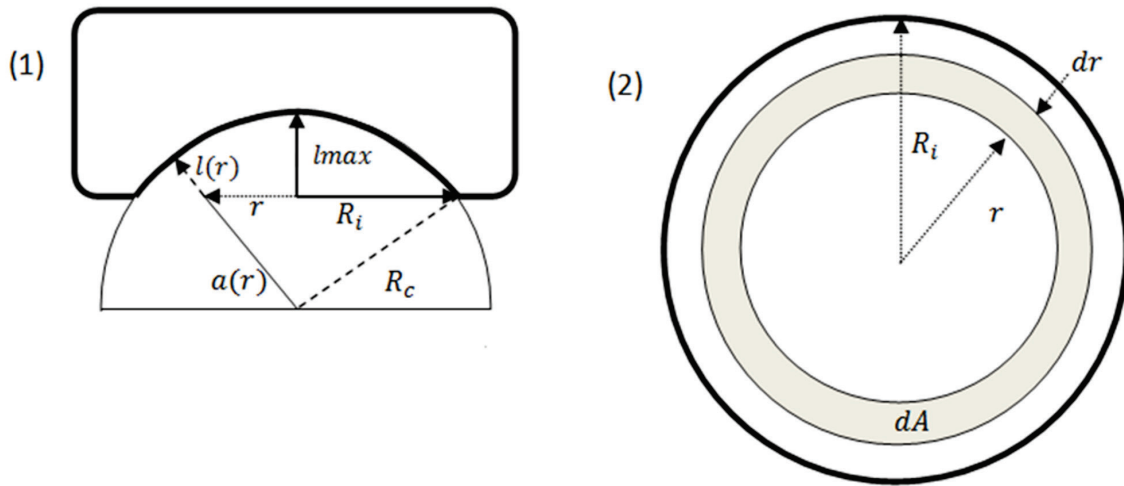
678



679

680 **Figure 8.** Product temperature distributions obtained from the contact area and curvature-  
 681 based distribution for a 5 % w/w sucrose solution processed at a shelf temperature of -25 °C  
 682 and four chamber pressures: (a) 4 Pa, (b) 6 Pa, (c) 9 Pa and (d) 15 Pa.

683



684

685 **Figure A.** Side (1) and top (2) view of the vial bottom represented as a semi-spherical calotte.

686

687

688